Transparent Yb^{3+} doped phosphate glass-ceramics

M. Hongisto[1], A. Veber[1], N.G. Boetti[2], S. Danto[3], V. Jubera[3], L. Petit[1]

[1] *Photonics Laboratory, Tampere University, Korkeakoulunkatu 3, 33720, Tampere, Finland.*

[2] *Fondazione LINKS – Leading Innovation & Knowledge for Society, Via P. C. Boggio 61, 10138 Torino, Italy*

[3] *CNRS, Univ. Bordeaux, Bordeaux INP, ICMCB, UMR 5026, F-33600 Pessac, France*

Abstract

Yb^{3+} doped oxyfluorophosphate glasses with the composition (98.75) [90NaPO$_3$-(10-x) Na$_2$O-xNaF] - 1.25Yb$_2$O$_3$ (in mol%) with x = 0, 2.5, 5, 7.5 and 10 were prepared using a standard melting process. The progressive replacement of Na$_2$O by NaF leads to an increase in the number of Q^2 units at the expense of the Q^1 units. This increase in the polymerization of the glass network leads to a shift of the optical band gap to lower wavelength, to a slight increase in the intensity of the emission at 1000 nm and more importantly to a change in the glass crystallization process. Indeed, both surface and bulk crystallization were observed in the glass with x = 0 while surface crystallization only occurs when NaF is added in the phosphate network. The heat treatment leads to the precipitation of at least three crystalline phases: as x increases, the NaPO$_3$ phase grows at the expense of Na$_5$P$_3$O$_{10}$. All glasses precipitate the Yb containing crystal, NaYbP$_2$O$_7$ which leads to an increase in the intensity of the emission at 1000 nm compared to the emission at 975 nm. We show for the first time to the best of our knowledge that transparent Yb^{3+} doped phosphate glass-ceramics can be obtained within this glass system when free of NaF.

Introduction

Materials doped with Yb^{3+} have been of great interest as Yb^{3+} has a very simple energy level structure consisting of the ground (^{2}F$_{7/2}$) and excited (^{2}F$_{5/2}$) states. As these two states are well separated, multiphonon relaxation and excited state absorption (ESA) are limited. Yb^{3+} doped materials can find applications in solid-state lasers [1], light emitting diodes [2], and more recently in solid-state laser induced cooling [3], just to cite a few examples. The Yb^{3+} doped materials can be pumped with wavelength in the range of ~0.9–1.0 μm using diode lasers, which are commercially available with high power. The emission then takes place in the ~1μm wavelength region. Additionally, the efficiency of Yb doped fiber is not degraded due to concentration

quenching and excited state absorption for example, as high Yb^{3+} doping can be used without a reduction of the upper-state lifetime.

Although silicate glasses remain the most commonly used glass hosts for Yb^{3+}, efforts have been focused for the past few decades on phosphate glasses due to their unique characteristics which can include, depending on their composition, low melting point, high thermal stability, high transparency, high gain density that is due to high solubility for lanthanide ions, low refractive index and low dispersion as compared to other glasses such as silicate glasses [4- 5]. Yb^{3+} ions in phosphate glasses can also possess high emission cross-section, broad absorption and emission band and long fluorescence lifetime (1-2 ms) [6]. Fluoride glasses are also good Yb^{3+} hosts due to their low phonon energy when compared with oxide glasses. However, their use is limited due to their poor mechanical and chemical resistance. Therefore, oxyfluoride glasses have been under investigation as they possess higher chemical stability and better mechanical properties than fluoride glasses and lower phonon energy than oxide glasses [7]. In addition, some oxyfluoride glasses can produce transparent glass-ceramics (GCs) containing fluorite nanocrystals after heat treatment [8].

A GC contains at least one type of functional crystalline phase and a residual glass. The first glass-ceramic (GC) was reported in the 1960s [9]. The GCs are usually prepared using a two-step process: the first step being the preparation of the glass. In the second step, the glass is heat treated under specific heating conditions in order to create the nuclei and to grow them into crystals. The heat treatment can lead to surface and/or volume precipitation of the crystals. To be considered as promising optical materials, the GCs should be composed of crystals homogeneously distributed in the volume glass matrix. The crystals should also contain the rare-earth ions in order to enhance the spectroscopic properties of the GCs compared to the parent glass [10]. Additionally, the GCs should also be transparent. Therefore, it is crucial to tailor both the crystal size and the refractive index difference between the crystals and the glass in order to minimize light scattering. Indeed, to ensure the optical transparency of the glass-ceramic, the size of the crystals needs to be smaller than the incident light wavelength [11]. The first transparent oxyfluoride glass-ceramic with enhanced luminescence properties was reported in 1993 [10].

The crystallization behavior of glasses within the system P_2O_5-SrO-Na_2O was reported in [12] and within the system P_2O_5-SrO-Na_2O-Al_2O_3-Y_2O_3-Yb_2O_3 in [13]. Although the heat treatment of the glasses in these systems leads to surface crystallization of multiple crystals, the

heat treatment of the Yb^{3+} doped glass within the system P_2O_5-SrO-Na_2O-Al_2O_3-Y_2O_3 leads to the precipitation of the $NaYbP_2O_7$ crystals increasing the excited state $^2F_{5/2}$ lifetime of Yb^{3+} and also the bandwidth of the Yb^{3+} emission band centered at 1 µm [13]. These changes in the spectroscopic properties induced by the precipitation of $NaYbP_2O_7$ crystals are in agreement with [14]. Indeed, the Yb^{3+}ions in $NaYbP_2O_7$ have typical fluorescence lifetime of 1-2 ms and a a broad emission band at room temperature, which is different from the typical luminescence of Yb^{3+} doped glasses [14].

Therefore, the goal of our study is to process new Yb^{3+} doped oxyfluoride glasses, in which crystals similar to the $NaYbP_2O_7$ ones would precipitate in the volume upon heat treatment. Here, new Yb^{3+}-doped oxyfluorophosphate glasses in the $NaPO_3$-Na_2O-NaF system were prepared and characterized. The study on the impact of replacing Na_2O with NaF on the physical, thermal, optical and structural properties of Yb^{3+} free glasses can be found in [15]. We first present the spectroscopic properties of the Yb^{3+} doped glasses in this system. Then, we discuss the changes in the optical properties induced by the heat treatment of the glasses.

Experimental

Glasses with the composition (98.75) [$90NaPO_3$-$(10-x)Na_2O$-xNaF] - 1.25 Yb_2O_3 (in mol%) with x = 0, 2.5, 5, 7.5 and 10 were prepared using the standard melt-quench method. The batches were prepared using $NaPO_3$ (Alfa Aesar, *tech.*), Na_2CO_3 (Sigma-Aldrich, *99.8%*), NaF (Sigma-Aldrich, *99.99%*) and Yb_2O_3 (Sigma-Aldrich, *99.9%*) as the raw materials. The glasses were melted in a Pt crucible for 5min between 950 and 975 °C, depending on the glass composition. After quenching, the glasses were annealed at 200 °C for 6 h to release the stress from the quench.

The Panalytical EMPYREAN multipurpose X-Ray Diffractometer with a iron filtered cobalt K_α radiation ($\lambda = 1.78897$ Å) was used to check that the as-prepared glasses were amorphous and to identify the phases present in the glass-ceramics. The data were collected from $2\Theta = 15°$-60° in 0.026° intervals. The glasses and heat treated glasses were crushed into powder and spread over a "zero-background holder" Si-plate for the measurement of the XRD spectra.

The density of the glasses were measured using Archimedes' method. Ethanol was used as the immersion liquid. The accuracy of the measurements are ±0.02 g/cm^3.

The thermal properties of the glasses, such as the glass transition temperature (T_g) and crystallization temperature (T_p) of the samples were measured using differential thermal analysis

(DTA) using the Netszch JUPITER F1 instrument. The measurements were carried out in a Pt crucible using a heating rate of 10 °C/min. The T_g was determined as the inflection point of the endotherm obtained by taking the first derivative of the DTA curve, while T_p was taken as the maximum peak of the exotherm. The onset of the crystallization peak, T_x, was also measured. All measurements were performed with an accuracy of ± 3 °C.

The absorption spectra of the polished glasses were measured using UV-Vis-NIR spectrophotometer (UV-3600 Plus, Shimadzu) from 250 to 1100 nm. The absorption cross-section σ_{abs} (λ) was calculated using Equation (1).

$$\sigma_{abs}(\lambda) = \frac{\ln 10 \ \log(I_0/I)}{NL} \tag{1}$$

where, $\log(I_0/I)$ is the absorbance, L the thickness of the sample (in cm) and N the concentration of rare-earth ions (ions/cm^3). The concentration of Yb^{3+} ions was calculated from the density of the glasses and expected composition. The accuracy of absorption cross-section determination was ±10%.

The emission spectra of the investigated glasses were measured from powder at room temperature using Spectro 320-131 Vis-NIR emission spectrometer (Instrument Systems, Germany). The excitation was achieved using a monochromatic single-mode fiber pigtailed laser diode (CM962UF76P-10R, Oclaro) temperature tuned to 960 nm in order to compare emission intensity between samples. Additionally, the shape of the emission was measured from the surface of the bulk glass using FLS1000, Edinburgh Instrument. The excitation was 900 nm. The shape of the emission was merged with emission intensity data in order to compare the emission shapes and intensities. The emission cross-section (σ_{emi}) of the investigated glasses was calculated using the equations [16]:

$$\sigma_{emi} = \frac{\lambda^4 A_R}{8\pi c n^2 \Delta\lambda_{eff}} \tag{2}$$

$$A_R = \frac{8\pi c n^2 (2J'+1)}{\lambda_p^4 (2J+1)} \int \sigma_{emi} d\lambda \tag{3}$$

where A_R is the spontaneous emission probability, $\int \sigma_{emi} d\lambda$ is the integrated emission cross section, $\Delta\lambda_{eff}$ the fluorescence effective linewidth, n is the refractive index of the medium expected to be ~1.54 [17], c is the speed of light, J', J are the total momentums for the upper and lower levels, respectively and λ_p is the absorption peak wavelength.

The effective bandwidth of the emission band ($\Delta\lambda_{eff}$) was calculated using the following equation:[16]

$$\Delta\lambda_{eff} = \int \frac{I(\lambda)d\lambda}{I_{max}} \tag{4}$$

where I (λ) is the emission intensity and I_{max} is the intensity at the peak wavelength λ_{max}.

The fluorescence lifetime of the $Yb^{3+}{:}^2F_{5/2}$ level was measured at room temperature. The measurements were performed at the very edge of the bulk glasses in order to minimize reabsorption using a light pulses of the 915 nm laser diode. The decay traces were fitted using single exponential. The detector (PDA10CS, Thorlabs) used for this measurement was equipped with a passband filter(FB980-10, Thorlabs). Estimated error of the lifetime measurement was ± 0.20 ms. The radiative lifetime (τ_{rad}) of the glasses were calculated using the following equation [18]:

$$\tau_{rad} = \frac{3\lambda^4}{32\pi cn^2 \int \sigma_{abs}(\lambda)d\lambda} \tag{5}$$

The integration is performed over the entire transition centered at λ_{max}.

The IR spectra were measured using a Perkin Elmer Spectrum One FTIR (Fourier-transform infrared spectroscopy) spectrometer in Attenuated Total Reflectance (ATR) mode in mid infrared region 650–1400 cm^{-1}. The resolution of the measurement was 1 cm^{-1} and the spectra were obtained from the accumulation of 8 scans. Additional IR measurements were performed with a Bruker Equinox 55 FTIR spectrometer in transmission mode from 1000 cm^{-1} to 5000 cm^{-1}. The resolution of these measurements was 2 cm^{-1} and the spectra was obtained from 32 scans performed in an inert atmosphere.

The Raman measurements were performed using Renishaw InVia Qontor Raman microscope, using a 532 nm laser for the excitation. The data were obtained with the accumulation of 3 scans.

Results and discussion

Structural and photoluminescence investigation

Glasses with the composition (98.75) [90NaPO$_3$-(10-x) Na$_2$O-xNaF] - 1.25 Yb$_2$O$_3$ (in mol%) with x = 0, 2.5, 5, 7.5 and 10 were successfully prepared. The impact of the replacement of Na$_2$O by NaF on the thermal, optical and structural properties of the Yb free glasses in the same glass system can be found in [15]. The changes in the glass composition has no impact on the density of the Yb^{3+} doped glasses (Table 1), which was consistent with the results reported in [15], where

similar results were observed without Yb^{3+}. Comparing the density of our doped glasses to that of the undoped ones reported in [15], the addition of Yb_2O_3 increases the density of the glass. As in [15], an increase in x decreases the T_g due to the presence of weaker ionic cross-linking between the modifier fluoride cations and non-bridging oxygen as suggested in [19]. One should point out that the glasses exhibit a ΔT, an empirical parameter often used for fiber drawing, greater than 90 °C, indicating that the investigated glasses have a good resistance towards crystallization [20].

The IR and Raman spectra of the glasses are presented in Figure 1a and b, respectively. They are similar to those of Yb^{3+} free glasses reported in [15]. The investigated glasses have a metaphosphate structure, free of Q^3 groups as suspected due to the absence of IR and Raman bands at 1300 cm^{-1}, typical of the $v(P=O)$ of Q^3 groups. A complete attribution of the IR and Raman bands can be found in [15]. The changes in the intensity of the IR and Raman bands with an increase in x are similar to those reported in [15] indicating that an increase in x in Yb containing glasses leads to an increase in the number of Q^2 units at the expense of Q^1 units. Also, the shift of the band gap to a lower wavelength is observed as x increases (Figure 2a). As seen in Figure 2b, the replacement of Na_2O by NaF has no impact on the shape of the absorption band of the Yb^{3+} 4f − 4f transition between $^2F_{7/2}$ and $^2F_{5/2}$ levels. The shape is similar to that of other Yb^{3+} doped fluorophosphate glasses [21]. As seen in Table 1, all glasses possess similar the absorption and emission cross-sections at 975 nm which are in a good agreement with the commercial QX-Kigre glass [22].

The normalized emission spectra are presented in Figure 3a. The emission band is typical of the emission of Yb^{3+} in an amorphous network. An increase of x decreases the intensity of the shoulder at ~1000 nm as compared to the main band at 975 nm, reducing the effective bandwidth of the emission band (Table 2). The changes in the shape of the Yb^{3+} emission may be related to radiation trapping and/or re-absorption as well as energy migration among the Yb^{3+} ions due an increase in the network connectivity [23]. As depicted in Figure 3b, an increase in x increases slightly the area of the emission band. The increase in the integral intensity of the emission with an increase in x can be related to the change in the network connectivity and also to the reduction in the number of OH^- groups, which are known quenchers of Yb^{3+} ions [24]. The OH content in the different glasses can be estimated from IR absorption spectrum (Figure 3c). The IR absorption spectra exhibit a broad band which can be related to the "free" OH groups (weakly associated) at 3500 cm^{-1} and to OH groups which are strongly associated at around 2800 ("strongly associated")

6

and 2350 cm^{-1} ("very strongly associated") [24]. As expected from the composition of the glasses, the absorption coefficient between 2250 and 3750 cm^{-1} is high indicating that the glasses are hygroscopic. Indeed, the richer the composition in P_2O_5 and in Na_2O, the more unstable the glass in atmospheric conditions [25]. Fluorine is often used as a drying agent to displace bound OH$^-$ - groups in the glass network [26], and thus an increase in x leads to a decrease in the intensity of the absorption bands related to the OH groups. We suspect that the addition of NaF at the expense of Na_2O increases the intensity of the Yb^{3+} emission as fewer OH$^-$ groups are present to quench the Yb^{3+} ions (Figure 3b).

The lifetime values of the Yb^{3+}:$^2F_{5/2}$ level are listed in Table 3. Within the accuracy of the measurement, all the glasses exhibit similar lifetime values which are comparable to those reported previously for phosphate glasses [13, 27] but longer than the lifetime reported in silicate [28] and tellurite [29-30]. As seen in Table 2, the measured lifetimes are less than the radiative lifetimes calculated using the Equation 5 either due to energy transfer among the Yb^{3+} ions (diffusion limited) [31] and/or direct coupling with OH$^-$ groups [23]. It is worth mentioning that no cooperative luminescence was detected from the investigated glasses indicating that there is no or very few Yb^{3+} clustering in the glass. Therefore, we suspect the short lifetime value to be due to the OH$^-$ groups in the glasses. We expect to be able to increase the lifetime values of the Yb^{3+}:$^2F_{5/2}$ level of the investigated glasses by reducing the OH$^-$ content in the glasses, possible either by heat treating the raw materials prior to melting, adding dehydration agent in the glass batch prior to the melting and/or melting the glasses under a reactive atmosphere such as suggested in [32].

In summary, the progressive replacement of Na_2O by NaF leads to a more polymerized phosphate network. This reduces the amount of OH$^-$ groups while having no significant impact on the site of Yb^{3+}.

Crystallization investigation

The crystallization properties of the investigated glasses were studied using different thermal treatments on a Pt foil in air, detailed in Table 4. First, the glasses were treated at (T_g+20 °C) for 17 h to form the nuclei and then at (T_p-40 °C) for 30 min to grow the nuclei into crystals. This is subsequently denoted as heat treatment A (HT-A). After heat treatment, the glasses are opaque which is a clear sign of crystallization. The surface of the HT-A glasses has a ceramic appearance after heat treatment while the inner part of the glasses exhibits a glassy appearance indicating that

surface crystallization dominates. Surface crystallization was confirmed using SEM. The images the heat treated glasses with x = 0, 5 and 7.5, taken as examples, are shown in (Figure 4). The SEM images were taken from the glasses polished from the side and with the surface at the top of the image to clearly image the surface crystallization. It can be seen that crystals with a needle like shape are growing perpendicular to the surface of the glass. The thickness of the crystallized layer decreases as x increases indicating that the progressive replacement of Na_2O by NaF reduces the crystallization tendency of the glasses. This is probably due to the increase in the glass connectivity with an increase in x as discussed above. Similar correlation between the crystallization tendency and network connectivity was reported in [13, 17]. According to the the Energy Dispersive Spectroscopy (EDS) mapping, Na rich crystals are expected in the glasses during the heat treatment.

In order to identify the crystals, the XRD pattern of the HT-A glasses were measured and can be found in Figure 5. The XRD pattern of heat treated glasses at (T_g+20 °C) for 17 h and then at T_p for 2 hours are also shown. This heat treatment was performed to fully crystallize the glasses and so to ease the identification of the crystals and is denoted as heat treatment B (HT-B). The XRD patterns show the presence of at least 3 crystalline phases: $NaPO_3$ [ICDD 00-011-0648], $Na_5P_3O_{10}$ [ICDD 00-011-0652 and 00-010-0179] and $NaYbP_2O_7$ [ICDD 04-014-6349]. As x increases, the $NaPO_3$ phase grows at the expense of $Na_5P_3O_{10}$ and a small amount of $Na_4P_4O_{12}(H_2O)$ is suspected to also partially transform into $NaH_2(PO_3)_4$.

The heat treatments A and B have an impact on the spectroscopic properties of Yb^{3+}. Changes not only in the shape of the emission but also in the area of the Yb^{3+} emission were noticed after heat treatment as depicted in Figures 6 and 3b, respectively. As seen in Figure 6, the heat treatment A increases the intensity of the shoulders at 1000, 1040 and 1055 nm as compared to the band at 975 nm leading to an increase of the bandwidth of the emission band (Table 2). One should point out that the changes in the shape of the emission after HT-A are less visible with an increase in x as less crystals precipitate when replacing Na_2O by NaF. A decrease in the area of the Yb^{3+} emission occurs after heat treatment, the decrease being more pronounced as x increases (Figure 3b). One should mention that the heat treatment A does not lead to changes in the Yb^{3+} excited state $^2F_{5/2}$ lifetime within the accuracy of the measurement although a reduction in the

8

lifetime is suspected to occur as the emission intensity decreased after the heat treatment, probably due to the reduction in the Yb-Yb distance (Table 3).

After the heat treatment B, the glasses exhibit lower overall emission areas compared to the as-prepared glasses (Figure 3b). Additionally, as illustrated in Figure 6, the position of the band at 975 nm shifts to 972 nm and the relative intensity of the shoulder at 1000 nm increases significantly leading to a decrease in the bandwidth of the emission band. Similar changes in the shape of the Yb^{3+} emission after heat treatment were reported in [13] and were related to the precipitation of Yb containing crystals. The change of the local Yb^{3+} environment is associated with a modification of the crystal field strength which explained both the shift of the zero-phonon line at 972 nm and the light modification of the $^2F_{7/2}$ fundamental multiplet splitting. One should point out that the emission spectra of the fully crystallized materials match well with the Yb^{3+} emission observed in $NaYbP_2O_7$ crystals [14]. This allows one to suggest that Yb^{3+} ions are mainly present in $NaYbP_2O_7$ and in the residual glassy phase.

Crystals with a needle-like shape as in Figure 7 were easily found in the volume of the heat treated glass with x = 0 while no crystals could be seen in the volume of the other heat treated glasses. Small crystals, visible as bright spots in Figure 7, can also seen in the SEM image. According to EDS analysis, the large, needle-like, crystals contain Na and P while the small crystals contain Yb. Therefore, these small crystals are thought to be $NaYb(P_2O_7)$. In order to check if the glass with x = 0 is the only glass exhibiting bulk crystallization, the XRD pattern of the glasses after heat treatment A were measured after polishing their surface to remove the crystals at the surface. Peaks with very small intensity were found only in the XRD pattern of the heat treated glass with x = 0 as depicted in Figure 8a confirming that the heat treatment leads to bulk and surface crystallization in the NaF-free glass and to only surface crystallization in the other glasses.

In order to check the possibility to control the crystallization of the glass with x = 0, this glass was heat treated at (T_g+20 °C) for 17 h and at (T_p-40 °C) for 1 hour, denoted as heat treatment C (HT-C), and at (T_g+20 °C) for 66 h and at (T_p-40 °C) for 30 min, denoted as heat treatment D (HT-D). As depicted in Figures 9, an increase of the heat treatment duration from 30 min to 1 hour at (T_p-40 °C) and from 17 h to 66 h at (T_g+20 °C) increases the size of the crystals from ~175 µm to ~250 µm and their number, respectively and so the intensity of the peaks in the XRD pattern,

especially for the HT-D glass (Figure 8a). According to the XRD pattern, we suspect the $Na_5P_3O_{10}$ I phase to precipitate in the volume of the glass. Based on the SEM image of the crystals found in the volume of the glass with x = 0, we also suspect the presence of $NaYbP_2O_7$ crystals in the glass. The amount of this phase is probably too small and/or too few to be detected with XRD. As seen in Figure 8b, the heat treated glasses after removing the surface layer are transparent confirming that it is possible to prepare Yb^{3+} doped transparent glass-ceramics with the $90NaPO_3$-10 Na_2O glass composition. The heat treated glasses have slightly lower transmittance compared to the as-prepared glass due to scattering caused by density fluctuations due to the presence of micro-crystals inside the glass matrix (Figure 8c). The transition between Yb^{3+} $^5F_{7/2}$ and $^2F_{5/2}$ energy levels is clearly visible. One should mention that the 3 transparent glass-ceramics obtained exhibit similar intensity and shape of emission (and so bandwidth) than the HT-A glass with x = 0 depicted in Figures 3b and 6a, respectively. Therefore, it is shown here that a heat treatment of the glass with x = 0 can be used to increase slightly the bandwidth of the emission band by increasing the intensity of the shoulder at 1µm while maintaining the spectral distribution of the emission.

Conclusion

In this study, novel Yb^{3+} doped glasses within the $NaPO_3$-Na_2O-NaF system were prepared and characterized. An increase in the NaF content at the expense of Na_2O leads to a polymerization of the glass network and so to changes in the crystallization process of the glass. All the glasses exhibit surface crystallization after heat treatment, the NaF-free glass being the only glass having also bulk crystallization .

We showed, for the first time to the best of our knowledge, that a heat-treatment of the glass with the $90NaPO_3$-10 Na_2O composition can produce transparent glass-ceramic with crystals also distributed in the volume of the glass. This transparent glass-ceramic was found to have a slightly larger bandwidth of the Yb^{3+} emission band than the as-prepared glass while having slightly lower intensity of the emission confirming that the newly developed glass–ceramic can be applicable in solid state lasers and other optical devices.

Acknowledgement

References

1. C. Hönninger, R. Paschotta, M. Graf, F. Morier-Genoud, G. Zhang, M. Moser, S. Biswal, J. Nees, A. Braun, G.A. Mourou, I. Johannsen, A. Giesen, W. Seeber, U. Keller, Ultrafast ytterbium-doped bulk lasers and laser amplifiers, Appl. Phys. B 69 (1999) 3–17

2. C.Zhu, J. Wang, M. Zhang, X. Ren, J. Shen, Y. Yue, Eu-, Tb-, and Dy-Doped Oxyfluoride Silicate Glasses for LED Applications, J. Am. Ceram. Soc. 97(3) (2014) 854–861

3. R.I. Epstein, M.I. Buchwald, B.C. Edwards, T.R. Gosnell, C.E Mungan, Observation of laser-induced fluorescent cooling of a solid, Nature 377 (1995) 500–502 (1995)

4. S. Jiang, M.J. Myers, D.L. Rhonehouse, S.J. Hamlin, J.D. Myers, U. Griebner, R. Koch, H. Schonnagel, Ytterbium-doped phosphate laser glasses, Proc. SPIE 2986 (1997) 10–15.

5. D. Pugliese, N.G. Boetti, J. Lousteau, E. Ceci-Ginistrelli, E. Bertone, F. Geobaldo, D. Milanese, Concentration quenching in an Er-doped phosphate glass for compact optical lasers and amplifiers, J. Alloys Compd. 657 (2016) 678–683.

6. D.W. Hughes, J.R.M. Bar, Laser diode pumped solid state lasers, J. Phys. (D). 25 (1992) 563.

7. M.C. Goncalves, L.F. Santos, R.M. Almeida, Rare-earth-doped transparent glass ceramics, C.R. Chim. 5 (2002) 845-854

8. H. Hayashi, S. Tanabe, T. Hanada, 1.4 µm band emission properties of Tm^{3+} ions in transparent glass ceramics containing PbF_2 nanocrystals for S-band amplifier, J. Appl. Phys. 89 (2001) 1041–1045

9. S.D. Stookey, S.D. Catalyzed crystallization of glass in theory and practice, Ind. Eng. Chem. 51 (1959) 805-808

10. Y. H. Wang and J. Ohwaki, New transparent vitroceramics codoped with Er^{3+} and Yb^{3+} for efficient frequency up-conversion, Appl. Phys. Lett. 63(24) (1993) 3268–3270

11. G. H. Beall, L. R. Pinckney, Nanophase glass-ceramics, J. Am. Ceram. Soc. 82(1) (1999) 5–1

12. J. Massera, M. Mayran, J. Rocherullé, L. Hupa, Crystallization behavior of phosphate glasses and its impact on the glasses' bioactivity, Journal of Material Science. 50 (2015) 3091-3102

13. R. Sen, N. N. G. Boetti, M. Hokka, L. Petit, Optical, structural and luminescence properties of oxyfluoride phosphate glasses and glass-ceramics doped with Yb^{3+}, Journal of Non Crystalline Solids: X 1 (2019) 100003

14. R. Ternane, M. Ferid, Y. Guyot, M. Trabelsi-Ayadi, G. Boulon, Spectroscopic properties of Yb^{3+} in $NaYbP_2O_7$ diphosphate single crystals, Journal of Alloys and Compounds 464 (2008) 327–331

15. N. Ojha, M. Tuomisto, M. Lastusaari, L. Petit, Upconversion from fluorophosphate glasses prepared with $NaYF_4$:Er^{3+},Yb^{3+} nanocrystals,. RSC Advances, 8 (2018) 19226 - 19236

16. C. Jiang, P. Deng, J. Zhang, G. Huang, F. Gan, Yb: tellurogermanate laser glass with high emission cross section, Journal of Luminescence 82 (1999) 321-326.

17. P. Lopez-Iscoa, L. Petit, J. Massera, D. Janner, N.G. Boetti, D. Pugliese, S. Fiorilli, C. Novara, F. Giorgis, D. Milanese, Effect of the addition of Al_2O_3, TiO_2 and ZnO on the thermal, structural and luminescence properties of Er^{3+}-doped phosphate glasses. Journal of Non-Crystalline Solids. 460 (2017) 161-168

18. M. J. Weber, J.E. Lynch, D.H. Blackburn, D. J. Cronin, Dependence of the Stimulated Emission Cross Section of Yb^{3+} on Host Glass Composition, IEEE J. Quantum Electron. QE-19 (1983) 1600-1608

19. Brauer, D. S., Anjum, M. N., Mneimne, M., Wilson, R. M., Doweidar, H., Hill, R. G. Fluoride-containing bioactive glass-ceramics. J. Non. Cryst. Solids. 358 (2012) 1438–1442

20. M. Çelikbilek, A.E. Ersundu, N. Solak, S. Aydın, Thermal and Microstructural Investigation of the TeO_2-WO_3 System. Journal of Alloys and Compounds. 509 (2011) 5646-5654.

21. J.H. Choi, A. Margaryan, A. Margaryan, F.G. Shi, Spectroscopic properties of Yb^{3+} in heavy metal contained fluorophosphate glasses. Mater. Res Bull 40 (2005) 2189–97.I

22. R. Koch, W.A. Clarkson, D.C. Hanna, S. Jiang, M.J. Myers, D. Rhonehouse, S.J. Hamlin, U. Griebner, H. Schonnagel, Opt. Commun. 134 (1997) 175.

23. K. Venkata Krishnaiah, R. Rajeswari, K. Upendra Kumar, S. Surendra Babu, I.R. Martín, C.K. Jayasankar, Spectroscopy and radiation trapping of Yb^{3+} ions in lead phosphate

glasses, J. Quant. Spectrosc. Radiat. Transfer 140 (2014) 37–47

24. H. Ohkawa, H. Hayashi, and Y. Kondo, Influence of water on non-radiative decay of Yb^{3+}–$^2F_{5/2}$ level in phosphate glass, Opt. Mater. 33(2) (2010) 128–130

25. G. Palavit, Phosphate glasses and water, Phosphorus Research Bulletin 6 (1996), 85 – 90

26. V. Nazabal, S. Todokori, A. Nukui, T. Matsumoto, S. Suehara, T. Hondo, T.Araki, S. Inoue, C. Rivero, and T. Cardinal, Oxyfluoride Tellurite Glasses Doped by Erbium: Thermal Analysis, Structural Organization and Spectral Properties,J. Non-Cryst. Solids, 325 (2003) 85–102

27. P. Nandi, G. Jose, Ytterbium-Doped P_2O_5-TeO_2 Glass for Laser Applications, IEEE J. Quantum Electron 42 (2006) 1115.

28. M. Cavillon, C. Kucera, T. W. Hawkins, N. Yu, P. Dragic, J. Ballato, Ytterbium-doped multicomponent fluorosilicate optical fibers with intrinsically low optical nonlinearities, Opc. Mat. Exp. 8(4) (2018) 745

29. X. Feng, C.H. Qi, F.Y. Lin, H.F. Hu, Tungsten–tellurite glass: a new candidate medium for Yb^{3+}-doping. J. Non-Cryst. Solids. 256 (1999) 372–377.

30. M.A.Merzliakov, V.V.Kouhar, G.E.Malashkevich, E.V.Pestryakov, Spectroscopy of Yb-doped tungsten–tellurite glass and assessment of its lasing properties glasses, Opt. Mat. 75 (2018) 142-149

31. V.Venkatramu, R.Vijaya, S.F.León-Luis, P.Babu, C.K.Jayasankar, V.Lavín, L.J.Dhareshwar, Optical properties of Yb^{3+}-doped phosphate laser glasses, J. Alloys Compds. 509 (2011) 5084–5089

32. P. Joshi, B. Richards, A. Jha, Reduction of OH⁻ ions in tellurite glasses using chlorine and oxygen gases, J. Mater. Res. 28(23) (2013) 3226

Table caption

Table 1: Physical and thermal properties of the investigated glasses, their absorption and coefficient and cross-section and their emission cross-section at 975 nm.

Table 2: Bandwidth of the emission band measured using a 900 nm excitation

Table 3: Excited state $^2F_{5/2}$ lifetime values of the glasses prior to and after heat treatment. Measurements were performed using laser excitation at 915 nm. Accuracy of measurement is ±0.20 ms.

Table 4: Different heat treatments used in this study.

Figure caption

Figure 1: IR (a) and Raman (b) spectra of the investigated glasses
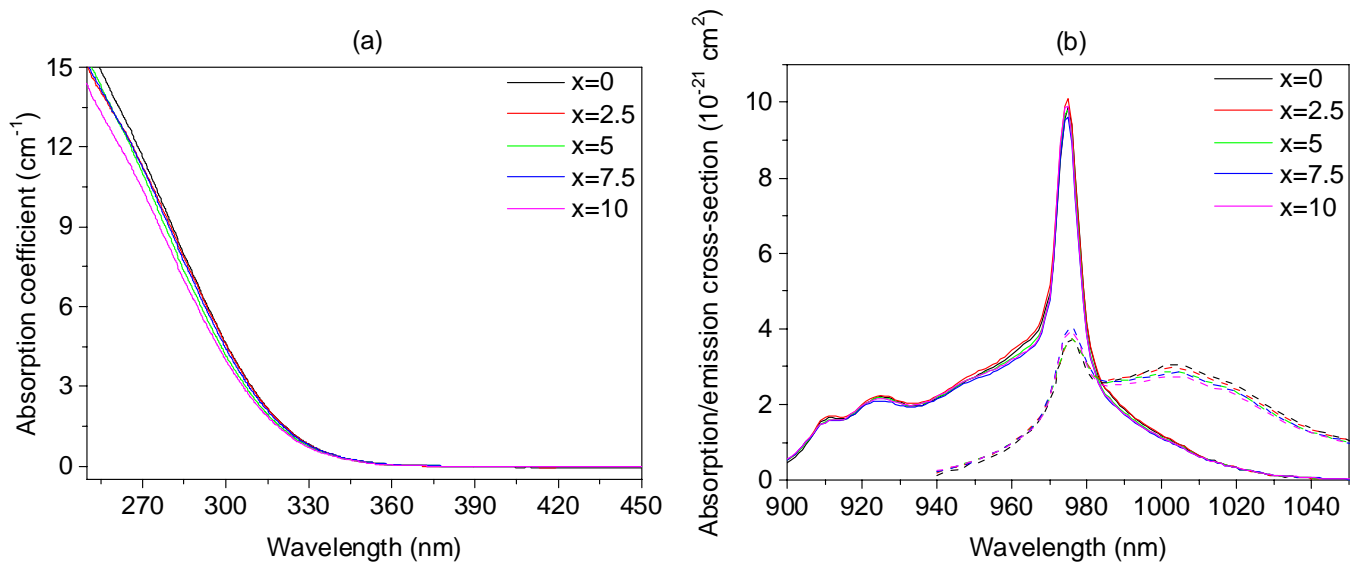
Figure 2: Absorption spectra (a) and absorption/emission (solid/dashed) cross sections centered at 975 nm (b) of the investigated glasses.
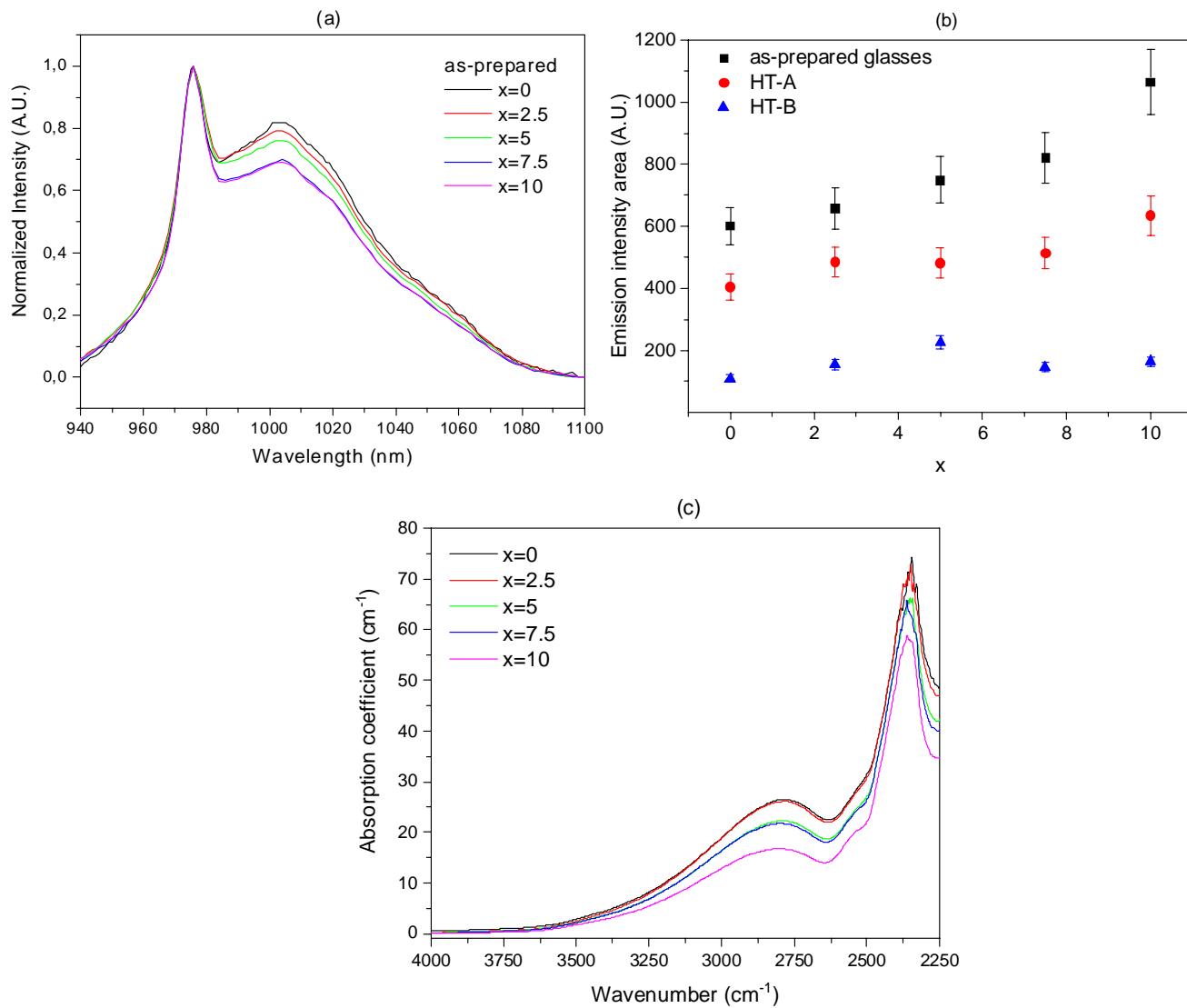
Figure 3: Emission spectra measured using a 900 nm excitation (a), integrated area of the emission band (b) and IR absorption spectra of the glasses (c)
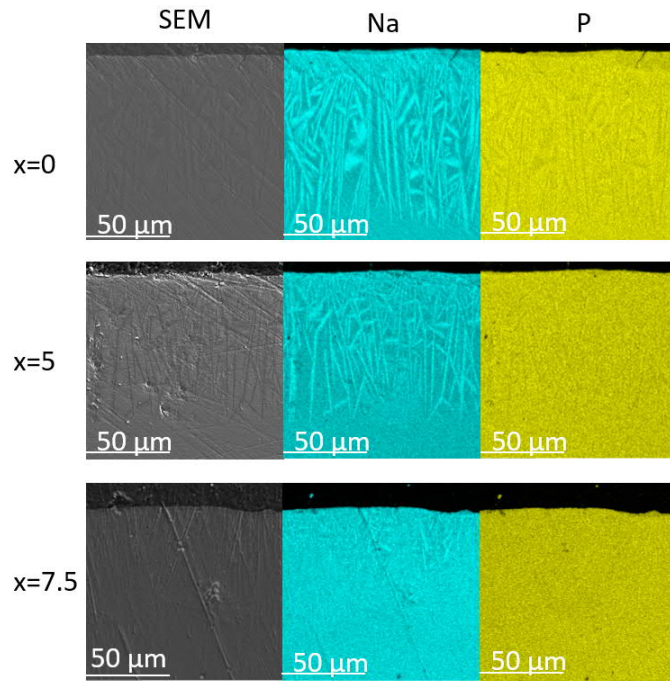
Figure 4: Elemental mapping of the crystals in the glasses' SEM images after heat treatment A
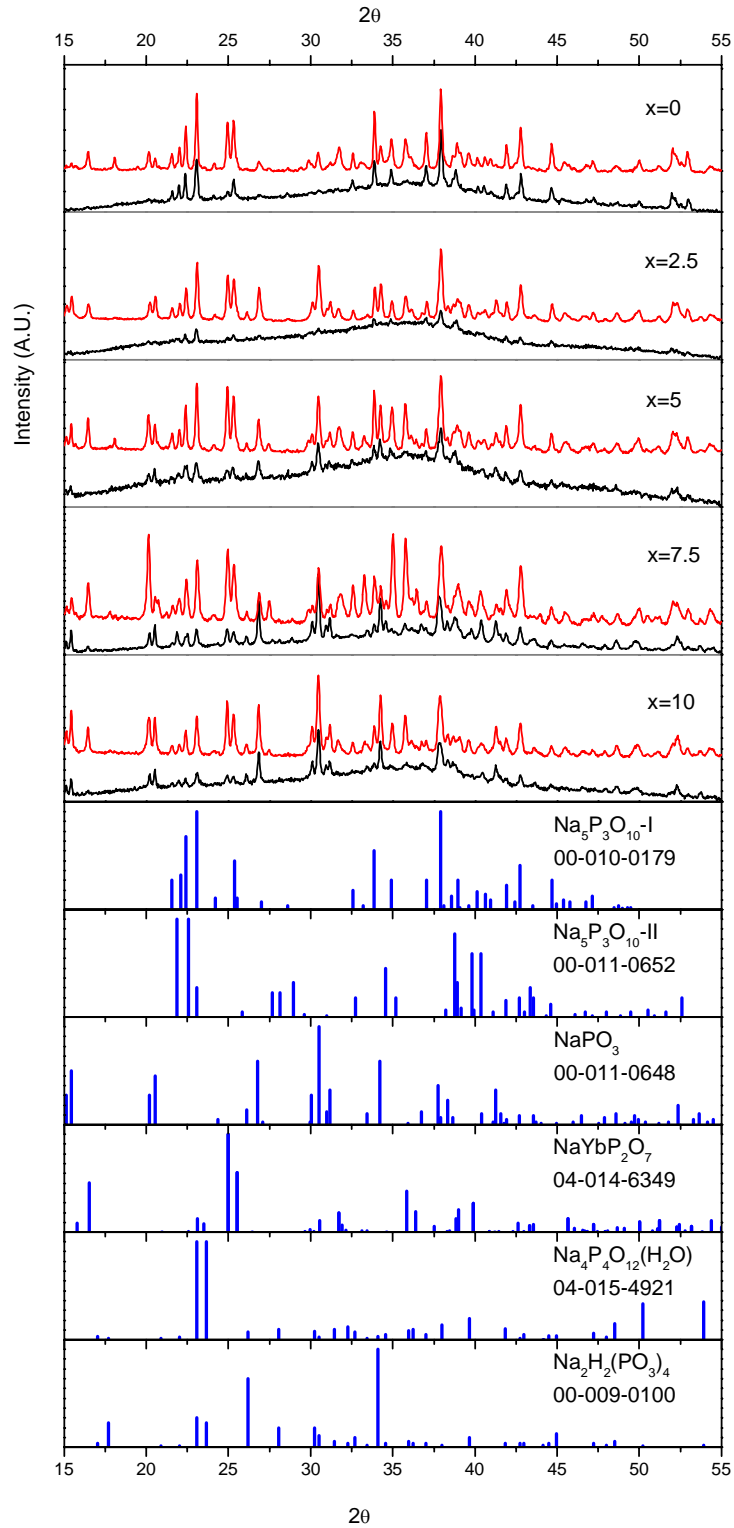
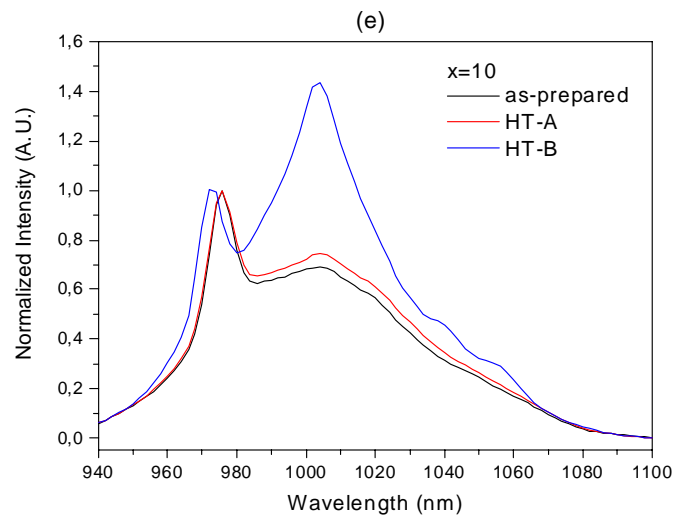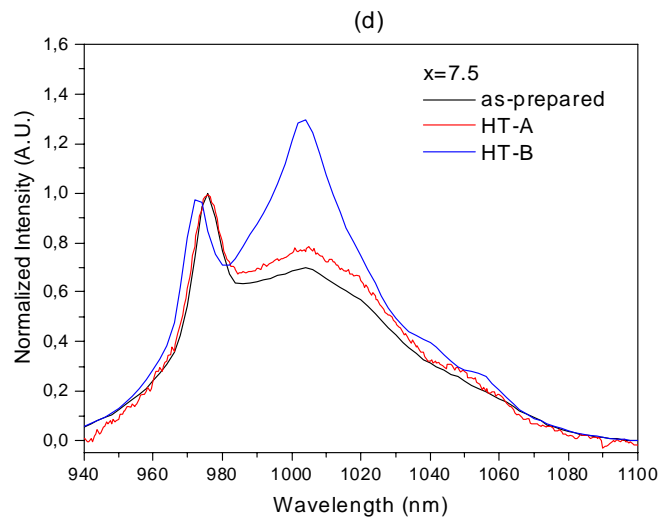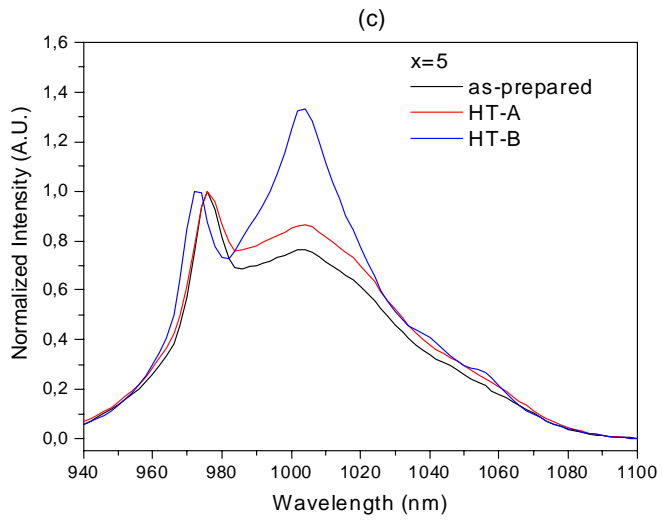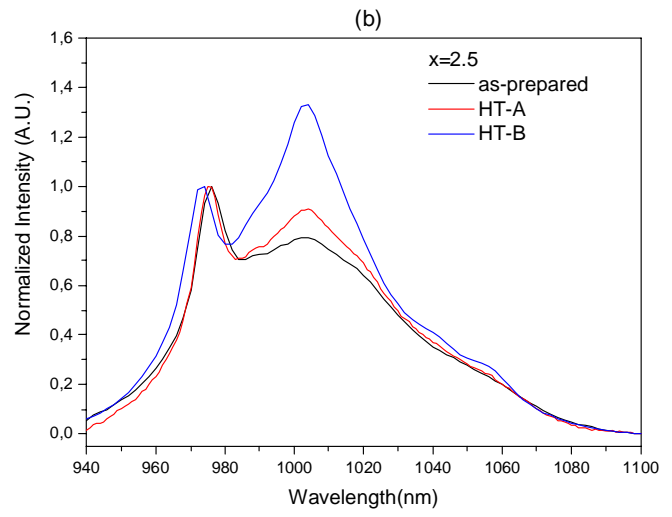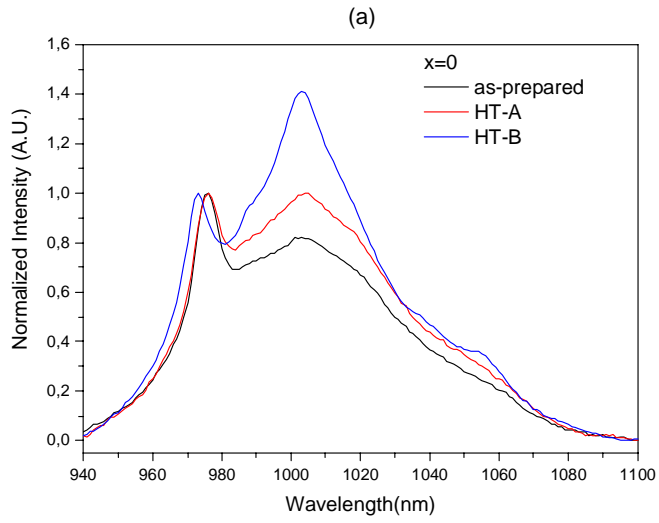**Figure 5:** XRD of the investigated glasses after heat treatment A (black), and B (red)

Figure 6: Normalized emission spectra of the glasses with (a) x = 0, (b) x = 2.5, (c) x = 5, (d) x = 7.5 and (d) x = 10 prior to and after heat treatment A or B. Excited at 900 nm.

Figure 7: SEM image of crystals found in the volume of the glass with x = 0 after heat treatment A

Figure 8: XRD patterns (also shown is the XRD pattern of $Na_5P_3O_{10}$-I [00-010-0179]) (a), the pictures (b) and the transmittance spectra (c) of heat treated glasses with x = 0

Figure 9: Optical images of the crystals found in the heat treated glasses with x = 0 after HT-A (a), HT-C (b) and HT-D (c). The images were taken with 5x microscope magnification in transmission mode using cross-polarized configuration of the microscope

Figure 1: IR (a) and Raman (b) spectra of the investigated glasses

Figure 2: Absorption spectra (a) and absorption/emission (solid/dashed) cross sections centered at 975 nm (b) of the investigated glasses.

Figure 3: Emission spectra measured using a 900 nm excitation (a), integrated area of the emission band (b) and IR absorption spectra of the glasses (c)

Figure 4: Elemental mapping of the crystals in the glasses' SEM images after heat treatment A

Figure 5: XRD of the investigated glasses after heat treatment A (black), and B (red)

(a)

(b)

(c)

(d)

(e)

20

Figure 6: Normalized emission spectra of the glasses with (a) x = 0, (b) x = 2.5, (c) x = 5, (d) x = 7.5 and (d) x = 10 prior to and after heat treatment A or B. Excited at 900 nm.
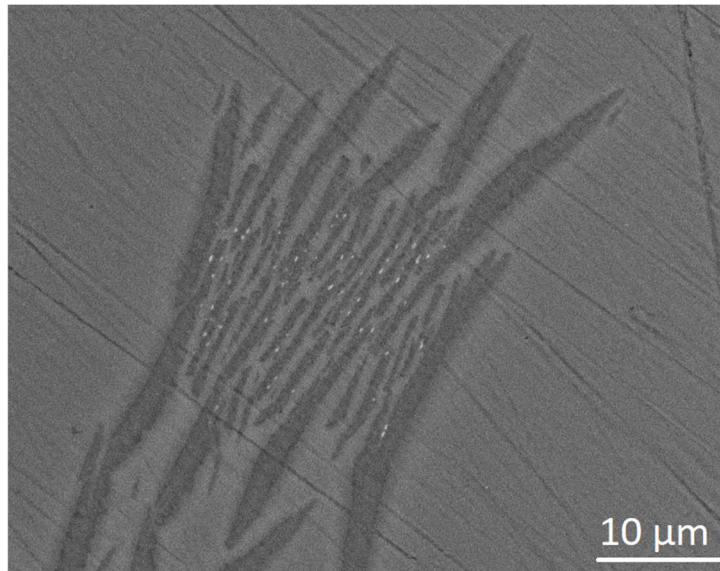
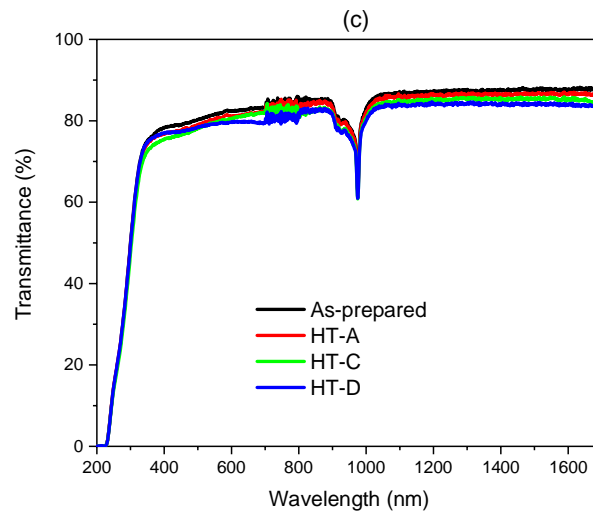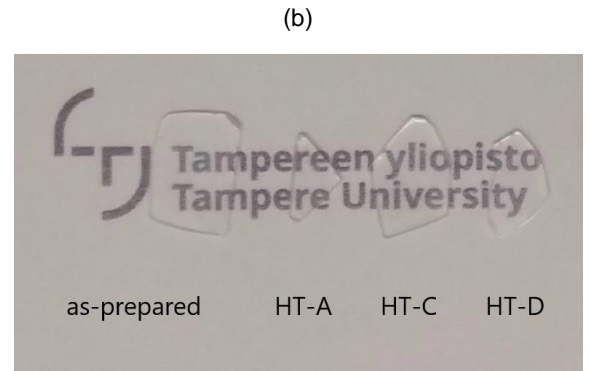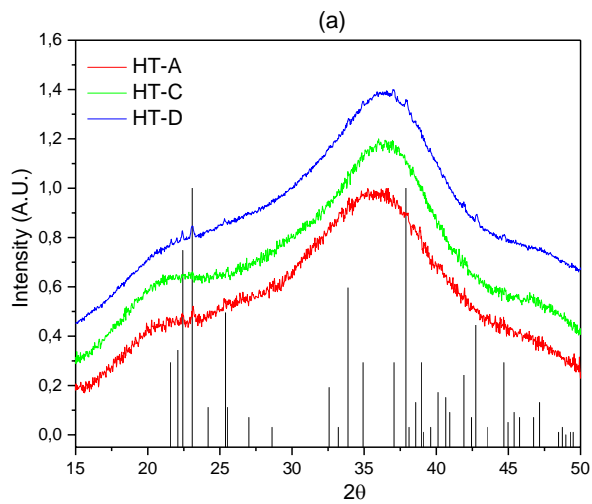**Figure 7:** SEM image of crystals found in the volume of the glass with x = 0 after heat treatment A

Figure 8: XRD patterns (also shown is the XRD pattern of $Na_5P_3O_{10}$-I [00-010-0179]) (a), the pictures (b) and the transmittance spectra (c) of heat treated glasses with x = 0
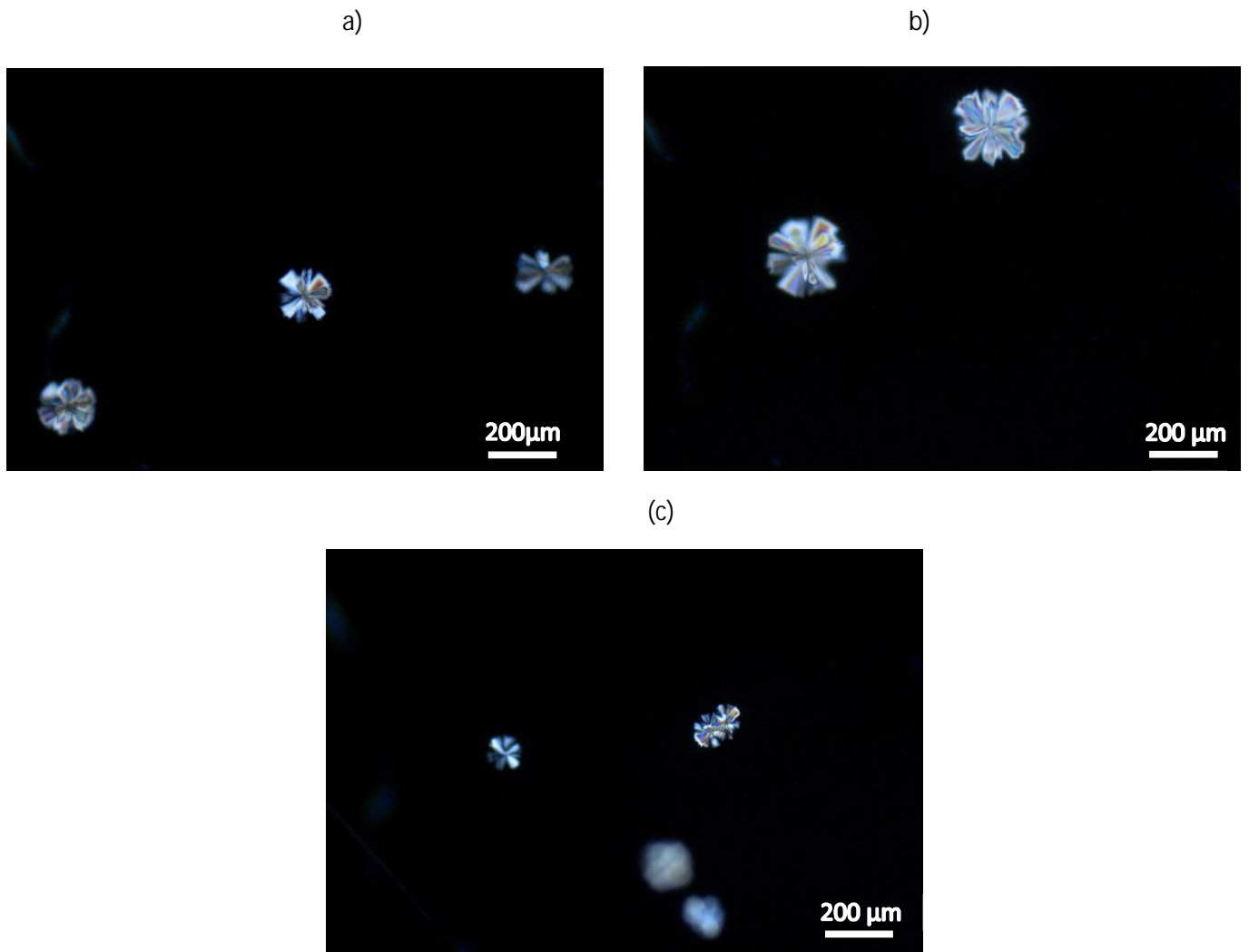
a)

b)

(c)

Figure 9: Optical images of the crystals found in the heat treated glasses with x = 0 after HT-A (a), HT-C (b) and HT-D (c). The images were taken with 5x microscope magnification in transmission mode using cross-polarized configuration of the microscope

Table 1: Physical and thermal properties of the investigated glasses, their absorption and coefficient and cross-section and their emission cross-section at 975 nm.

x	ρ (g.cm^{-3}) ± 0.02 g.cm^{-3}	T_g (°C) ± 3°C	T_x (°C) ± 3°C	T_p (°C) ± 3°C	$\Delta T = T_x - T_g$ (°C) ± 6°C	Yb^{3+} (ions·cm^{-3}) (10^{20}) ± 5%	α_{abs} (cm^{-1}) at 975 nm	σ_{abs} at 975 nm (10^{-21}cm^2) ± 10%	σ_{emi} at 975 nm (10^{-21}cm^2)
0	2.63	299	389	417	90	3.89	3.84	9.87	3.72
2.5	2.61	295	394	413	99	3.88	3.92	10.10	3.76
5	2.62	293	396	418	103	3.92	3.84	9.81	3.77
7.5	2.62	289	379	407	90	3.93	3.79	9.63	4.09
10	2.63	291	386	418	95	3.97	3.93	9.90	3.98

Table 2: Bandwidth of the emission band measured using a 900 nm excitation

x	As-prepared glasses (nm)	Heat treatment A (nm)	Heat treatment B (nm)
0	63	73	60
2.5	63	65	58
5	61	67	57
7.5	56	65	57
10	56	60	57

Table 3: Excited state $^2F_{5/2}$ lifetime values of the glasses prior to and after heat treatment. Measurements were performed using laser excitation at 915 nm. Accuracy of measurement is ±0.20 ms.

x	Calculated lifetime (ms)	Measured lifetime (±0.20 ms)	
		As-prepared glasses (ms)	Heat treatment A (ms)
0	1.8	1.1	0.8
2.5	1.7	0.9	0.6
5	1.9	0.9	0.9
7.5	1.8	0.8	0.6
10	1.9	0.8	0.7

Table 4: Different heat treatments used in this study.

HT	Nucleation phase	Growth phase
A	T_g + 20ºC for 17h	T_p - 40ºC for 30min
B	T_g + 20ºC for 17h	T_p for 2h
C	T_g + 20ºC for 17h	T_p - 40ºC for 1h
D	T_g + 20ºC for 66h	T_p - 40ºC for 30min